crystals

MDPI

Article

A Study on the Growth Window of Polycrystalline Diamond on Si_3N_4-coated N-Polar GaN

Mohamadali Malakoutian [1], Matthew A. Laurent [1] and Srabanti Chowdhury [1,2,*]

[1] Department of Electrical and Computer Engineering, University of California, Davis, CA 95616, USA; malakoutian@ucdavis.edu (M.M.); matlaurent@gmail.com (M.A.L.)
[2] Department of Electrical Engineering, Stanford University, Stanford, CA 94305, USA
* Correspondence: srabanti@stanford.edu

Received: 29 August 2019; Accepted: 24 September 2019; Published: 25 September 2019

Abstract: Diamond has the most desirable thermal properties for applications in electronics. In principle, diamond is the best candidate for integration with other materials for thermal management due to its high thermal conductivity. Therefore, if low thermal boundary resistance can be developed between diamond and the semiconductor material, it would most effectively channel the heat away from areas of high power dissipation. Recent advancement of N-polar GaN in high power RF and conventional power electronics motivated us to study the diamond/Si_3N_4/GaN interface to understand how effectively the heat can be transferred from the GaN channel to diamond heat-sink. Prior studies showed that there are challenges in incorporating diamond with GaN while still maintaining the high crystalline quality necessary to observe the desirable thermal properties of the material. Therefore, in this study we investigated the influence of methane concentration (0.5–6%), gas pressure (40–90 Torr), sample surface temperature (600–850 °C), and growth duration (1~5 h) on polycrystalline diamond growth. The diamond/Si_3N_4/GaN interface looks abrupt with no signs of etching of the GaN for the samples with methane concentration above 2%, pressures up to 90 Torr, and temperatures < 850 °C, allowing for incorporation of diamond close to the active region of the device. This approach contrasts with most prior research, which require surface roughening and thick growth on the backside.

Keywords: polycrystalline diamond growth; N-polar GaN; thermal management; active device cooling; stress analysis

1. Introduction

Diamond has a number of excellent properties such as the highest known thermal conductivity (TC), wide energy bandgap, high electron and hole mobility, widest optical transparency window, and chemical inertness, which make it a unique solid-state material and desirable for several technological applications. The high TC provides strong motivation for integrating diamond into electronic devices for thermal management purposes [1]. In addition to high TC, diamond is electrically insulating compared with other high TC materials (e.g., copper), which makes diamond a better choice for low dielectric loss needed applications such as gallium nitride (GaN)-based power devices [2].

Gallium nitride is a wide-bandgap semiconductor which has shown great promise in high power, high frequency, and high temperature applications for electronics. This is due to favorable material properties such as large breakdown field, high electron saturation velocity, and high charge concentration [3–5]. Most of the research in the field of electronic devices is focused on the Ga-polar direction of the GaN (GaN[0001]) [6,7]. However, high electron mobility transistors (HEMTs) with N-polar GaN (GaN$[000\bar{1}]$) exhibit advantages in both enhancement and depletion (deep recessed structure) modes and offer higher scalability, lower resistivity Ohmic contacts, lower gate capacitance,

and more effective back barrier, which can result in a larger transconductance (g_m), drain saturation current (I_{Dsat}), cutoff frequency (f_t), and maximum frequency (f_{max}) [8–10].

N-polar GaN HEMTs can deliver powers in W-band frequencies more than 3-fold of the state-of-the-art Ga-polar GaN HEMTs [11]. Even though using SiC as the substrate for these HEMT structures provides adequate TC to keep individual device temperatures within an acceptable range, these transistors are still running close to the thermal budget of other components within the packaged module, so these devices cannot be operated at maximum possible power and frequency, as will be required for future applications. Furthermore, high temperatures (self-heating) in the channel decreases the carrier mobility ($\propto T^{-3/2}$) and degrades the device performance, which eventually decreases the reliability and lifetime of the device [12–15]. Therefore, it is necessary to dissipate the generated heat from the top or bottom of the device. Owing to the excellent TC of diamond (>2000 W/m.K), it can be used for heat spreading into the heat-sinks in GaN-based HEMTs. The heat dissipation can be done through the substrate by replacing the substrate with diamond using growth or wafer bonding on the backside of the HEMT structure [16–18]. The other approach is to grow polycrystalline diamond on the top of the device, which can be much closer to the high temperature spot in the channel (5–20 nm) and may be more effective than the former approach. Others have reported direct diamond growth on AlGaN/GaN HEMTs, however these focused on Ga-polar GaN for the HEMT structure [19–22]. In this work, we were focused on the integration of diamond into N-polar GaN with a goal of improving HEMT technology.

Polycrystalline diamond was grown using a microwave plasma chemical vapor deposition (MPCVD) system. Different MPCVD reactor structures reported in [23–25] all utilize hydrogen and methane (CH_4) gases as the main reactants. Hydrogen atoms are necessary to break C-H bonds and provide CH_3^+ to the surface for diamond growth and also promote the formation of diamond over graphite by making the graphite to diamond conversion energy lower [2]. Since a hydrogen plasma is the main species in diamond growth chamber, high temperature combined with hydrogen gas and H^+ radicals can cause the decomposition and etching of the GaN layer. Damaging the GaN layer can change the properties of the 2-dimensional electron gas (2DEG) and in some serious cases can remove it completely. In order to protect the GaN layer, a thin layer of Si_3N_4 can be used for surface protection. This is compatible with most state-of-the-art N-polar GaN HEMT fabrication processes, which use Si_3N_4 as gate dielectric and surface passivation. A thin Si_3N_4 layer reduces TC of the whole structure, while on the other hand, improves thermal boundary resistance (TBR) between diamond and GaN by more than 70% [26]. Therefore, Si_3N_4 can fill a beneficial role for both electronic and thermal properties. However, making the Si_3N_4 layer as thin as possible is crucial to make the heat dissipation more efficient and avoid the low bulk TC of Si_3N_4. In this work, we used a 20 nm in situ Si_3N_4 grown by metalorganic chemical vapor deposition (MOCVD) on top of N-polar GaN. Using Si_3N_4 for Ga-polar GaN protection during diamond growth was reported by [22,26–28]. It is important to point out that MOCVD grown Si_3N_4 shows distinctively different surface properties compared to ex situ depositions like plasma-enhanced chemical vapor deposition (PECVD) or low-pressure chemical vapor deposition (LPCVD).

Our motivation for studying diamond growth on Si_3N_4/N-polar GaN layer stack is dedicated to technological applications. N-polar GaN transistors are currently at the forefront of research for high-power-density RF devices with one of their advantages being superior gate control due to the proximity of the channel to the semiconductor surface. This combination of factors (high power density and channel proximity to surface) makes the N-polar GaN HEMT an excellent candidate to benefit from diamond integration as a heat spreader on top. However, a transistor is incomplete almost for any application without an appropriate dielectric layer. Here we chose Si_3N_4 since N-polar GaN RF devices typically use Si_3N_4 as its dielectric. Therefore, growth on the dielectric surface closely models the use case we have plan for.

As mentioned earlier, single-crystalline diamond has the largest TC among all known bulk materials, while polycrystalline diamonds exhibit much smaller TC which is also usually anisotropic in

layers thinner than 10 µm [29,30]. However, according to reported results by Angadi et al., which shows the relationship between diamond TC and grain size, a diamond layer with grain sizes larger than 400 nm can be more efficient than GaN for heat dissipation purposes [31]. Phase purity as one of the key parameters plays a critical role in integration of diamond into foreign substrates. Having impurities, non-diamond carbons, and defects reduces the diamond phase purity and affect the TC of the film [32]. In order to increase the TC of polycrystalline diamond, the phase purity (sp^3/sp^2 bonding ratio) of the film needs to be as close as possible to that of single-crystalline diamond (~100%) and the average grain size must be maximized. In this paper, the effect of diamond growth parameters (i.e., CH_4%, pressure, temperature, and time) on the average grain size, thickness, diamond/Si_3N_4/GaN interface, and diamond phase purity were investigated under growth conditions that do not damage the underlying GaN. The film's residual stress, as an important mechanical property of diamond, is also reported with respect to the different growth parameters.

2. Materials and Methods

A 2" sapphire wafer with ~ 1.5 µm semi insulating N-polar GaN layer and 20 nm MOCVD Si_3N_4 on top was used as the substrate for this systematic growth study of diamond. The GaN and Si_3N_4 layers were grown by MOCVD on sapphire substrates in a Thomas Swan close-coupled showerhead reactor [33,34]. The wafer was cut into 5×5 mm^2 pieces before seeding for polycrystalline diamond growth. In this study, a polymer-assisted dip seeding technique was used with 30 min of poly (diallyldimethylammonium chloride) solution dipping time to make the surface electrostatically positive (zeta potential ≈ +50 mV) and then 30 min of oxygen-terminated diamond nanoparticles (NPs) dipping with about −50 mV zeta potential. Due to the large difference between the surface of the sample and NPs in potential, the seeding process was self-assembly and gave a high density of NPs on the surface (>10^{12} cm^{-2}). After the NPs dipping, samples were rinsed with water and dried with N_2 gas. This seeding method was originally developed on silicon substrate by [35]. However, as the surface properties of Si_3N_4/GaN and Si are different, although we adapted the seeding method described in [35], we did a significant amount of original work to develop our polymer-based seeding method for Si_3N_4/N-polar GaN substrates to achieve the highest possible NP density on the surface. Our systematic study on optimizing the NP seeding of Ga-polar GaN, N-polar GaN, and Si_3N_4/N-polar GaN substrates is described in [36].

The NP suspension used for seeding was purchased from Adamas Nanotechnologies (Raleigh, NC, USA) and was specified as monodispersed diamond NPs at 1 wt% in deionized (DI) water. The particles had an average size of 5 nm with a −50 mV Zeta potential. The poly(diallyldimethylammonium chloride) solution, or PDDAC, with 2 wt% in DI water was purchased from Sigma Aldrich (St. Louis, MO, USA).

After the seeding, the samples placed inside an SDS 5000 series microwave plasma CVD reactor from Seki Diamond Systems (Tokyo, Japan) for growth. For the study, a standard low power baseline recipe was used; 2% CH_4/H_2, 1600 W plasma power, 40 torr pressure, 600 °C temperature, and 1-h growth time. Each growth parameter was changed individually while keeping others constant: CH_4 content was varied from 0.5% to 6%, pressure was varied from 40 to 90 torr, temperature was varied from 600 to 850 °C, and time was varied from 1 to 5 h. The temperature of the substrate was measured during the growth using a dual wavelength optical pyrometer (Williamson Pro DWF-24-40-CCCC, Williamson corporation, Concord, MA, USA). After the growth, the samples were cooled down to room temperature in H_2 plasma to prevent any non-diamond material formation on the surface.

The samples were characterized by scanning electron microscopy (SEM—FEI Nova NanoSEM 430, FEI, Hillsboro, OR, USA) in plan- and cross-sectional views to assess the grain size, film uniformity, layer thickness, and study the diamond/Si_3N_4/GaN interface. The samples were also characterized by a Raman spectroscopy system (RM1000, 514 nm argon laser, Renishaw, West Dundee, IL, USA) to assess the crystalline quality with respect to its phase purity by measuring the relative sp^3/sp^2 bonding ratio and film stress by measuring the peak shift from single crystalline diamond.

3. Results and Discussion

3.1. Grain Size and Thickness

In the first set of experiments, the CH_4% in the gas mixture was changed (CH_4/H_2 = 0.5–6%) while keeping the other growth conditions constant. The plan-view SEM micrographs of the grown diamond with different CH_4 content are shown in Figure 1. When the CH_4 content was 0.5%, grown diamond layer showed non-uniformity with voids. This confirmed that the CH_4 content was not high enough to form a uniform layer in one hour and the growth process was mass transport limited. In the case of 1% CH_4, the diamond layer exhibited a larger density of nano-crystalline diamonds (NCDs) with a smaller number of voids. Above 2% CH_4 (3, 5 and 6%) the layer was completely uniform, and the crystallite density was not changing, which was the sign of surface reaction limited growth. At this stage, the growth mode was a combination of island growth (Volmer-Weber mode) and layer growth (Frank-van der Merwe mode) [37]. The uniform distribution of diamond grains with a negligible size variation was a confirmation of the uniformity in seeding and nucleation prior to growth. The average grain size of the diamond layer with 0.5, 1, 2, 3, 5 and 6% CH_4 contents was 90, 102, 113, 111, 108 and 112 nm, respectively. The average grain size increased with variation in CH_4 from 0.5 to 2% due to the larger lateral crystallite expansion rate, while it remained constant around 110 nm above 2% CH_4 as the lateral crystallite expansion rate saturated around 110 nm/h. Sternschulte et al. reported similar trend with CH_4% as the growth mode changed from mass transport limited to surface reaction limited [38]. Another possible reason for the lateral crystallite expansion rate saturation above 2% CH_4 (beside surface reaction limited growth) was the increased re-nucleation rate of the diamond.

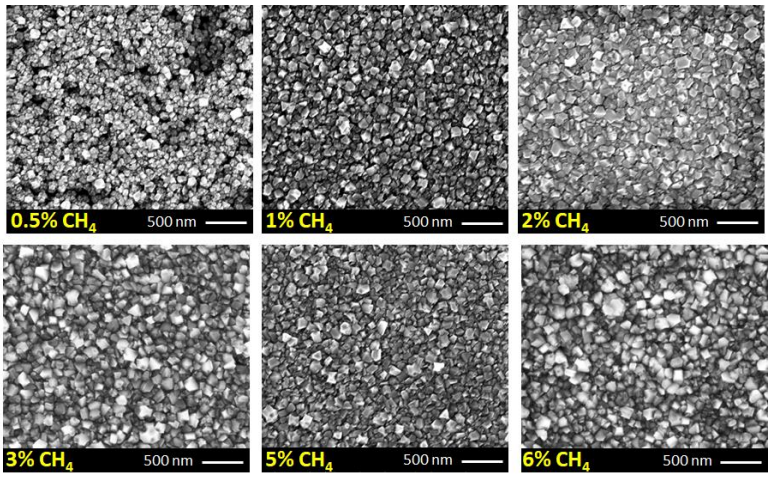

Figure 1. The effect of CH_4 content in the gas mixture on film uniformity and grain size (plan-view SEM micrographs).

Figure 2 shows the cross-sectional SEM micrographs of the samples. There are several etch pits and roughening signs in the diamond/Si_3N_4/GaN interface in the case of 0.5% CH_4 content. The number of etch signs decreased drastically by increasing the CH_4 content to 1%, and above 2% no etch signs were observed in the interface of diamond/Si_3N_4/GaN. These results suggest that in order to have an abrupt interface, it is crucial to increase the CH_4 content to or above 2% at the early stages of the growth.

In the second set of experiments, the effect of the pressure was investigated (40 ~ 90 Torr with 10 Torr steps). In order to keep the temperature constant (~ 600 °C) for all the growths, the microwave power was varied from 1200 to 1600 W. Figure 3 shows the plan-view and cross-sectional view SEMs of the samples. Both the grain size and thickness of the diamond layer increased with pressure. Increasing the pressure, increases the plasma density over the surface and provides more radicals/reactants for the growth. The change in the grain size and thickness with respect to the pressure is shown in Figure 3e. Both the grain size and thickness appear to have a super-linear (parabolic, R^2 = 0.9976) relationship

with the pressure. The grain size increased from 113 nm at 40 Torr, to 409 nm at 90 Torr. The thickness changed from 130 to 590 nm when the pressure varied from 40 to 90 Torr. With increasing pressure, the growth rate increases due to the higher plasma density and more energetic reactants in the chamber. However, the thickness increases more rapidly than the average grain size, which suggest that the higher pressure enhances the vertical growth rate more than the lateral crystallite expansion rate. As shown in the inset of Figure 3e, at the onset of growth the grains start to expand by coalescing or dominating smaller grains during the growth [39]. As the layer growth proceeds, the smallest grains are buried by larger grains. The rate at which this happens, and the maximum size of crystallites which can be achieved for a fixed growth time (1 h in this case) is influenced by the growth parameters.

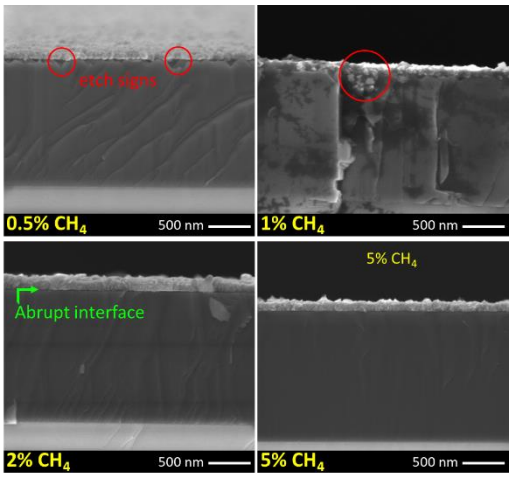

Figure 2. CH_4 content effect on the interface of the diamond/Si_3N_4/GaN (cross-sectional SEMs).

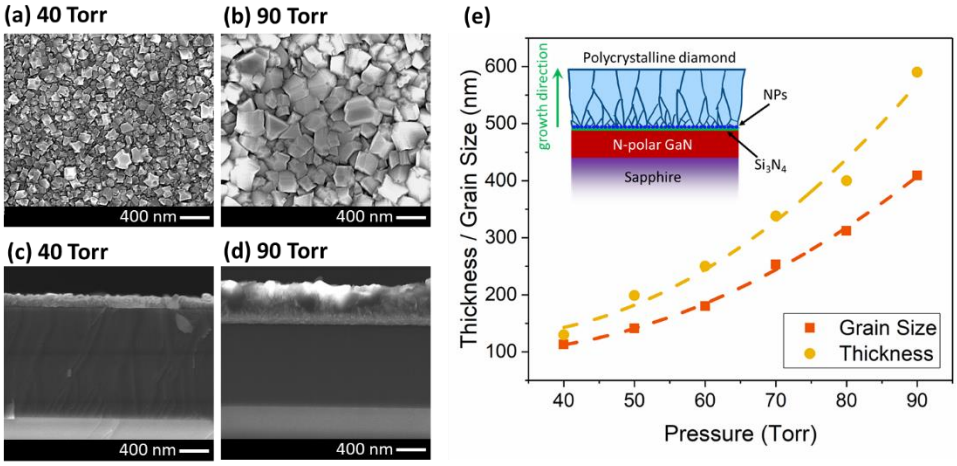

Figure 3. Plan- and cross-sectional-view SEMs of the diamond layer at (**a**,**c**) 40 and (**b**,**d**) 90 Torr. (**e**) The relationship between thickness/grain size and the pressure (lines are guides to the eye only). (Inset figure) Schematic cross-section of the sample after diamond growth.

As can be seen in Figure 3c,d, the cross-sectional view SEMs at 40 and 90 Torr pressures, the diamond/Si_3N_4/GaN interface of all samples looks abrupt with no etching or roughening of the substrate. The SEM micrographs for other pressures between 50 to 80 Torr also look abrupt at the interface. This data confirmed that increasing the pressure does not affect the etching process if there are enough radicals or reactants at the surface to immediately begin the diamond-phase nucleation on the seed layer and protect the underlying layer.

In the third set of experiments, pressure and microwave power were adjusted simultaneously to change the temperature from 600 to 850 °C with 50 °C steps. The grain size increased from 113 nm at 600 °C, to 419 nm at 850 °C (Figure 4a–c). The thickness changed from 130 to 696 nm when the

temperature varied from 600 to 850 °C (Figure 4d–f). Figure 4g shows that the grain size and also the thickness of the diamond increased by temperature with a parabolic behavior (R^2 = 0.9990). The thickness increased more rapidly than the average grain size. This is possibly due to the very high density seeding (>10^{12} cm^{-2}) on the sample surface. Growing diamond using hydrogen plasma (as opposed to Ar-rich plasma) is another reason for having higher vertical growth rate. It is worthy to note that the diamond/Si_3N_4/GaN interface was abrupt with no etching between 600 to 850 °C for all the samples. This makes the growth recipe suitable for integration with epitaxial GaN for electronic devices like HEMTs.

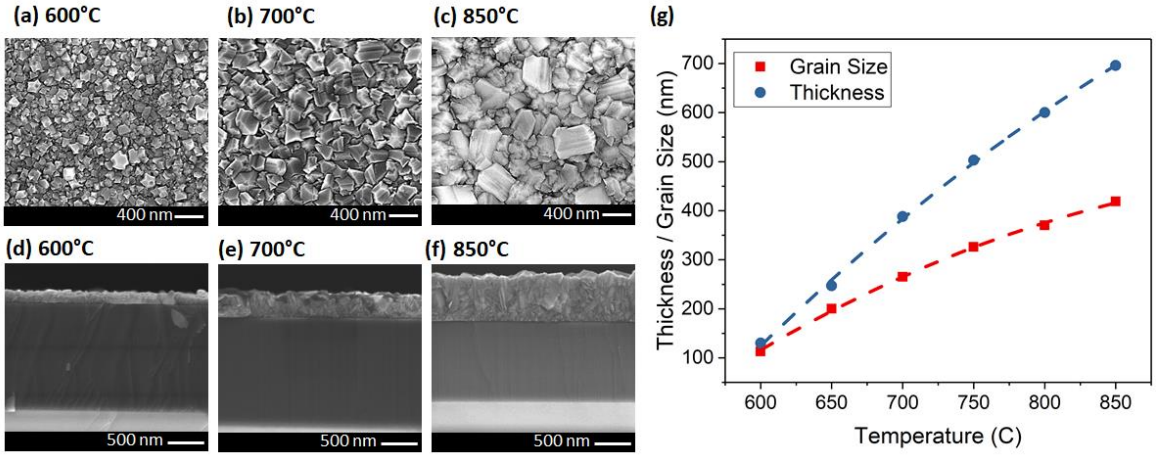

Figure 4. Plan- and cross-sectional-view SEMs of the diamond layer at (**a**,**d**) 600, (**b**,**e**) 700 and (**c**,**f**) 850 °C. (**g**) The relationship between thickness/grain size and the temperature (lines are guides to the eye only).

In the last set of experiments, the growth time was increased in steps from 1 to 5 h for constant growth parameters. The SEM micrographs of the samples are shown in Figure 5. The grain size of the diamond increased from 113 nm in one hour to 550 nm in 5 h growth. Zou et al. also reported a grain size between 500 to 800 nm after 5 h growth in the 600–700 °C temperature range. They used a 120 nm Si_3N_4 as protection layer on Ga-polar GaN to maintain an abrupt interface [27]. In another work, Zhou et al. reported growth of polycrystalline diamond at 650 °C, which resulted in 150–650 nm grain sizes on top of 50 nm Si_3N_4. They measured a TC in the range of 55 to 320 W/m·K which increased with increasing grain size [22].

In our growth time series, the crystal grain faceting did not change, which was expected since the chamber thermodynamics were invariant across this series. This was unlike the temperature study, in which increasing the temperature changed thermodynamic condition of the chamber, which resulted in a shape change of the grains from particle-like (with 111 facets) toward more flat surfaces (with larger 100 facets) (Figure 4a–c). The thickness increased from 130 to 794 nm for one- and 5-h growths, respectively. The grain size and thickness appeared to have a super-linear relationship with time up to 3 h and then changed to a sublinear relationship (Figure 5g). The difference between the grain size and thickness increased with time, which was due to the higher vertical growth rate in our samples. We may be able to control the growth rate along the different axis by changing the NPs seeding density and the nucleation recipe. However, the growth conditions which promote lateral versus vertical growth rates and their correlation to crystallite shapes are still under investigation.

In the case of 5 h growth, partial delamination of the diamond layer was observed from the surface during the cooling cycle at the end of the recipe. We believe this was caused by the large compressive stress in sapphire wafer during the cooling cycle, which was also reported by others [21,40]. This issue elaborated upon more in the next section.

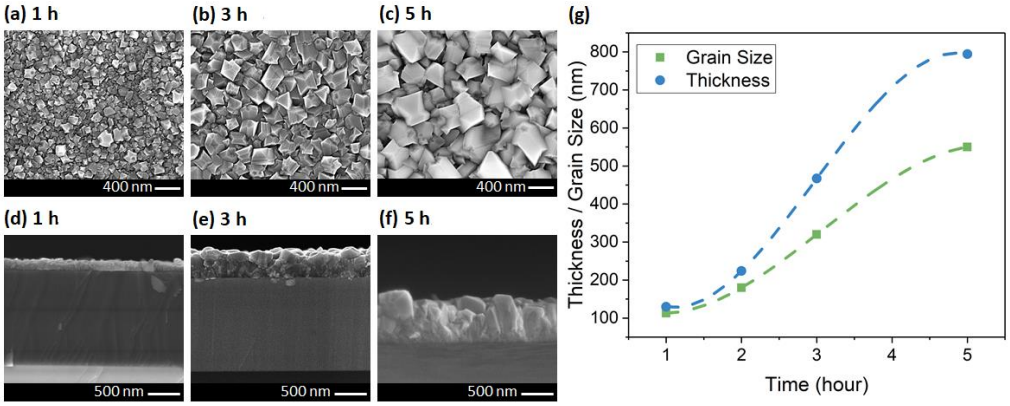

Figure 5. Plan- and cross-sectional-view SEMs of the diamond layer at (**a**,**d**) 1, (**b**,**e**) 3, and (**c**,**f**) 5 h. (**g**) The relationship between thickness/grain size and the growth time (lines are guides to the eye only).

3.2. Phase Purity and Residual Stress

In order to determine the phase purity and stress of the diamond layer, Raman spectroscopy with a 514 nm laser wavelength was used. The Raman spectra of the grown diamond at different CH_4 contents (0.5 ~ 6%) are shown in Figure 6. The diamond peak (or sp^3 bonding signature ~ 1332 cm^{-1}) was strengthened by increasing the CH_4%. The shift and broadening of the diamond peak in nanocrystalline diamond can be explained by quantum confinement effect [41]. The other non-diamond peaks also increased due to the formation of amorphous graphite at around 1560 to 1600 cm^{-1}. Some other peaks are visible in the spectra, 1140 and 1450 cm^{-1}, which corresponds to C-H bonding and polyacetylene. The increase in the intensity of these two peaks by increasing CH_4% was due to the re-nucleation process, which resulted in smaller grains and more polyacetylene between the grain boundaries [42]. The sharper intensity of diamond peak than the other peaks indicated the higher proportion of sp^3 carbon atoms in these samples. By increasing CH_4%, the relative intensity of broad G-peak increased, and the G-band slightly moved up to higher frequencies (~1580 cm^{-1}). The slight shift in the G-peak frequency was due to the carbon soot formation and increase in the amorphous carbon component [43].

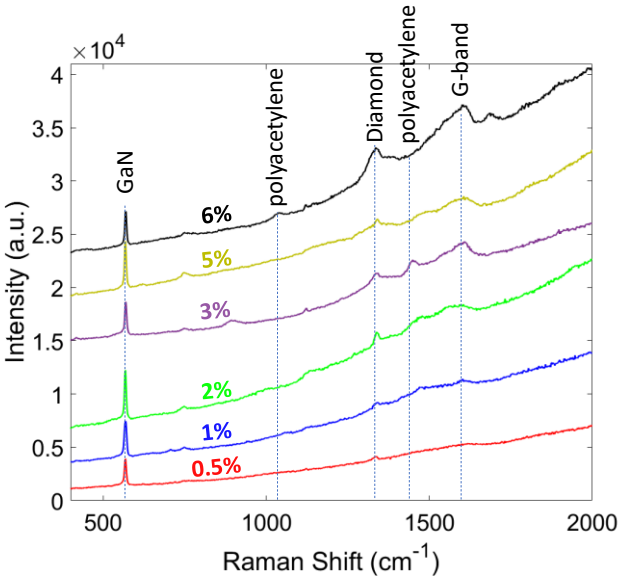

Figure 6. Raman spectra of the diamond films grown at different CH_4 content.

Having higher CH_4% in the gas mixture resulted in a higher C_xH_y radical content in the plasma. These radicals assist the nucleation process, but simultaneously enhance the re-nucleation rate of the diamond and also increase the sp^2 formation. Eckert et al. demonstrated via Monte Carlo simulation

that having lower CH_4% decreases C_4H_2 and C_3H_2 radicals and makes C_2H_2, CH_2, and CH_3 the only available radicals for C-C bonding. This eventually results in a lower sp^2 nucleation, which is desirable for achieving high TC and large grain size in diamond films [44]. Another method to decrease sp^2 content in the film is increasing the temperature and pressure of the hydrogen plasma, which results in a more aggressive environment, and enhances the etching process of sp^2 carbons by atomic hydrogen.

The phase purity (sp^3/sp^2 ratio) of the diamond layer can be calculated using Equation (1):

$$PP = (75 \times A_d)/(75 \times A_d + \sum A_{nd}) \times 100\%, \quad (1)$$

where, PP is the phase purity, A_d is the diamond peak area, which was fitted with a Lorentz profile, $\sum A_{nd}$ is the sum of all non-diamond peaks area including D- and G-peaks, which were fitted with a Gaussian profile [45]. The reason for having a correction factor of 75 is due to the more effective Raman scattering of sp^2 than sp^3 carbon bonding [46,47]. As shown in Table 1, increasing CH_4% resulted in a higher diamond phase purity (79.71% at 0.5% CH_4 to 94.36% at 6% CH_4) due to the stronger diamond peak.

The residual stress of the diamond film plays a critical role in determination of diamond delamination from the substrate. It includes thermal and intrinsic stress. Thermal stress is caused by the difference in the coefficient of thermal expansion (CTE) between diamond (~1.1 µm/m.K) and Si_3N_4/GaN/sapphire substrate (~3.3/4.1/5.5 µm/m.K) during the cooling cycle from growth temperature (600 ~ 850 °C) to room temperature. Since the substrate has a much larger CTE than diamond, it shrinks more after post-growth cooling and applies a large compressive stress to diamond film. Intrinsic stress is due to the incorporation of impurities and defect formation [48]. The bi-axial residual stress is proportional to Raman shift as explained in [48,49] and can be calculated using Equation (2):

$$\Sigma = -0.567(\vartheta_m - \vartheta_0)\ (GPa), \quad (2)$$

where, ϑ_m is the Raman frequency of the measured peak, and ϑ_0=1332 cm^{-1} is the Raman peak frequency with no residual stress [49]. The negative value for σ results from a compressive stress and positive value corresponds to a tensile stress. Table 1 shows that all the samples with varying CH_4 gas phase content exhibited a compressive stress. The stress magnitude increased from 3.4 to 5.2 GPa at 0.5% and 5% CH_4, respectively, due to the increase in the thickness. The residual stress magnitude for 6% CH_4 decreased to 4.9 GPa, which can be due to the increase in the re-nucleation rate and film relaxation by ultra-nano-crystalline diamond (UNCD) formation. More grain boundaries and polyacetylene result in a tensile stress in the film, which can compensate a portion of the compressive stress caused by CTE mismatch [45]. This conclusion needs further investigation.

Table 1. Grain size, thickness, Raman peak, phase purity, and stress of diamond at different CH_4%.

CH_4 (%)	Grain Size (nm)	Thickness (nm)	ϑ_m (cm^{-1})	PP (%)	Stress (GPa)
0.5	90	85	1337.9	79.71	−3.4
1	102	116	1339.0	85.15	−4.0
2	113	130	1339.5	90.1	−4.2
3	111	135	1340.3	90.84	−4.7
5	108	146	1341.1	93.11	−5.2
6	112	159	1340.6	94.36	−4.9

The Raman spectra for the second set of experiments, where the growth pressure was changing from 40 to 90 Torr with 10 Torr steps, are shown in Figure 7. It can be seen that by increasing the pressure the relative intensity of the diamond peak increases with respect to other non-diamond peaks (sp^3/sp^2 ratio). As a result, the phase purity of the diamond film changed from 90.1% at 40 Torr to 97.98% at 90 Torr (Table 2). The residual stress of the diamond film showed a compressive nature and increased with the pressure due to the increase in the thickness. Increasing the pressure, decreased

the formation of sp^2 bonding carbons suggesting a decrease in compressive stress, while increasing the thickness and grain size applied a larger compressive stress. In this study, up to 90 Torr pressure, we observed no delamination from the substrate.

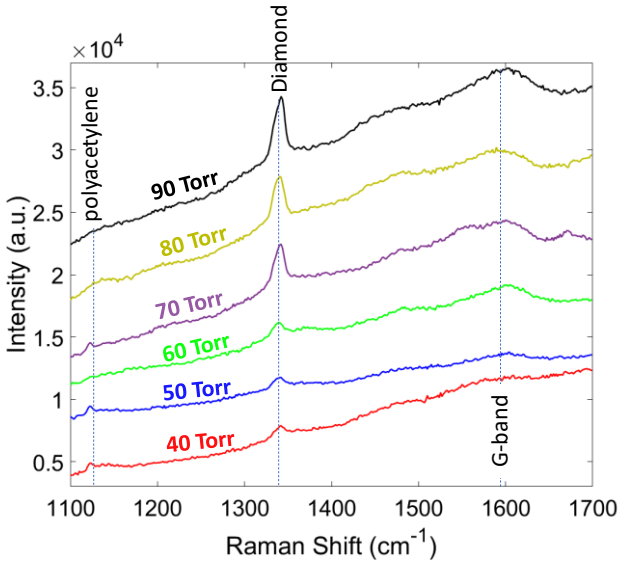

Figure 7. Raman spectra of the diamond films grown at different pressures.

Table 2. Grain size, thickness, Raman peak, phase purity, and stress of diamond at different pressures.

Pressure (Torr)	Grain Size (nm)	Thickness (nm)	ϑ_m (cm^{-1})	PP (%)	Stress (GPa)
40	113	130	1339.5	90.1	−4.2
50	141	199	1340.0	91.59	−4.5
60	180	250	1340.7	92.13	−4.9
70	253	338	1341.6	94.52	−5.4
80	312	400	1341.9	96.81	−5.6
90	409	590	1342.1	97.98	−5.7

In Figure 8, the Raman spectra of the diamond films grown at different temperatures (600 to 850 °C with 50 °C steps) are shown. The intensity of the diamond peak increased with temperature as expected due to a higher growth rate, which resulted in larger grain size and thickness. The sp^3/sp^2 ratio increased by the temperature and polyacetylene peaks (~1140 and 1450 cm^{-1}) disappeared at 850 °C. The phase purity of the diamond film compared at different temperatures and are shown in Table 3. The phase purity increased from 90.1% at 600 °C to 98.57% at 850 °C, which is very close to single crystalline diamond value at 100%. The residual stress in the diamond films are shown in Table 3. The residual stress showed a compressive nature and the magnitude increased from 4.2 at 600 °C to 6.3 at 850 °C. Similar to pressure study results, the increase in the thickness is the main reason for larger compressive stress. In this study, up to 850 °C we observed no delamination of the diamond film from the substrate.

Table 3. Grain size, thickness, Raman peak, phase purity, and stress of diamond at different temperatures.

Temperature (°C)	Grain Size (nm)	Thickness (nm)	ϑ_m (cm^{-1})	PP (%)	Stress (GPa)
600	113	130	1339.5	90.1	−4.2
650	200	247	1340.8	92.22	−5.0
700	265	388	1341.5	96.11	−5.4
750	326	503	1342.4	96.79	−5.9
800	370	600	1342.7	98.16	−6.1
850	419	696	1343.1	98.57	−6.3

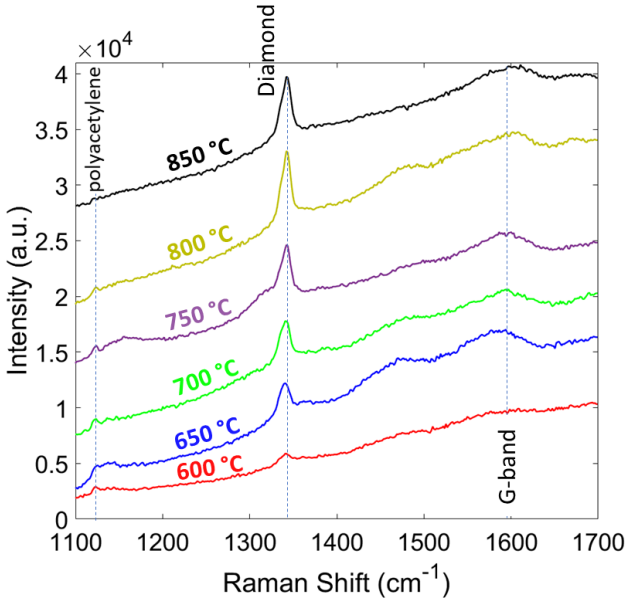

Figure 8. Raman spectra of the diamond films grown at different temperatures.

The last set of experiments were focused on the growth duration from 1 to 5 h. Figure 9 shows the diamond peak strengthens with increasing growth time, which corresponds to a larger ratio of sp^3 to sp^2 carbon bonding. The longer growth duration resulted in a higher phase purity as indicated in Table 4. It also can be seen from Table 4 that the residual stress increased with the time, due to the larger grain size and thickness of the diamond film. In the case of 5 h, about 70% of the sample area was delaminated from the substrate, which was due to the large compressive stress (−7.1 GPa). The delamination issue can be solved by roughening the surface prior to the nucleation stage, to enhance the adhesion of the diamond layer or by finding ways to mitigate film stress.

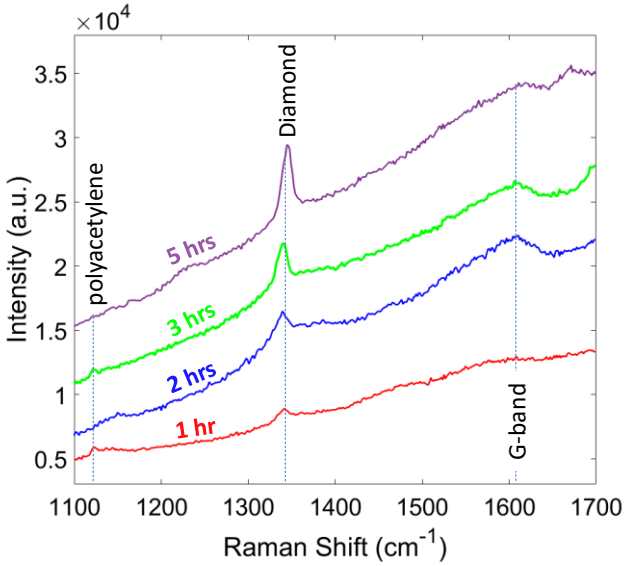

Figure 9. Raman spectra of the diamond films for different growth times.

Table 4. Grain size, thickness, Raman peak, phase purity, and stress of diamond for different growth durations.

Time (h)	Grain Size (nm)	Thickness (nm)	ϑ_m (cm^{-1})	PP (%)	Stress (GPa)
1	113	130	1339.5	90.1	−4.2
2	180	224	1340.2	93.61	−4.6
3	320	467	1342.1	95.22	−5.7
5	550	794	1344.6	98.84	−7.1

The results of this study are summarized in Figure 10a,b, which show the phase purity versus grain size and residual stress versus thickness of all the samples, respectively. As shown in Figure 10a, the phase purity increased with the average grain size of polycrystalline diamond up to 400 nm and then saturated above this point at 98.84%. The magnitude of compressive residual stress in the diamond film (Figure 10b), increased with the thickness and showed a linear relationship. The only datapoints that do not follow the main trend in these two plots belong to the CH_4 content study, which suggests that changing CH_4% may apply an offset to the graphs.

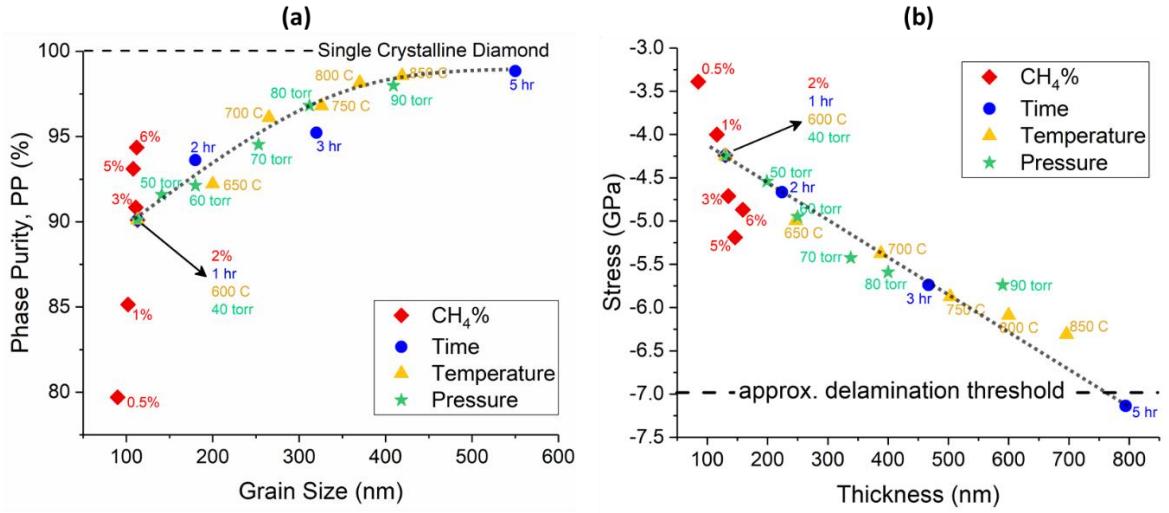

Figure 10. (**a**) Phase purity versus grain size of the diamond layer. (**b**) Residual stress as a function of film thickness. lines are guides to the eye only, for both of the figures.

4. Conclusions

A systematic study on the growth of polycrystalline diamond was performed on Si_3N_4-coated N-polar GaN substrates in a wide range of growth parameters (CH_4 concentration 0.5–6%, pressure 40–90 Torr, temperature 600–850 °C, and time 1–5 h). The CVD-grown diamonds were compared using SEM and Raman spectroscopy with respect to their grain size, thickness, interface abruptness, phase purity, and residual stress. It has been shown that using 2% or more CH_4 content decreases the etching signs at the diamond/Si_3N_4/GaN interface and exhibits a better abruptness. Changing other parameters (pressure, temperature, and time) did not affect the interface as long as there was enough CH_4 in the gas mixture to make a uniform nucleation layer at the beginning of the growth for Si_3N_4/GaN protection (etching prevention). The phase purity of diamond varies between 79.71 and 98.84% for 90 and 550 nm grain size, respectively. The residual compressive stress depends mostly on the thickness and changes from −3.4 GPa at 85 nm to −7.1 GPa at 794 nm film thickness. SiC formation at the diamond/Si_3N_4 interface provides a robust chemical bonding to the substrate and prevents delamination even at a high residual stress (up to 7 GPa compressive stress). The higher compressive stress in the diamond layer (above 7 GPa) may result in delamination from the substrate. This may be resolved by techniques like adding a re-nucleation layer in the middle of the growth to relax the entire layer or provide tensile stress, which requires further investigation. The results of this study

suggest a wide growth window of polycrystalline diamond on Si_3N_4/GaN with bulk-like properties, while demonstrating its compatibility with N-polar GaN HEMT technology and fabrication process.

Author Contributions: S.C. and M.A.L. conceived the topic discussed in this paper; M.M. synthesized the material; M.M. performed the experiments and the microscopic study; M.M., M.A.L. and S.C., designed the experiments and conceptualized the manuscript, M.M. primarily wrote the main manuscript text; M.A.L. and S.C. modified the manuscript. All authors have given approval to the final version of the manuscript.

Funding: This research was funded by Semiconductor Research Corporation under ComSenTer (JUMP) program.

Acknowledgments: We would like to thank Prof. Mishra's group at University of California Santa Barbara for providing N-polar GaN wafers.

Conflicts of Interest: The authors declare no conflict of interest.

References

1. Davies, G. Basic Properties of Diamond: Phonon Spectra, Thermal Properties, Band Structure. In *CVD Diamond for Electronic Devices and Sensors*; Sussmann, R.S., Ed.; John Wiley & Sons Ltd: West Sussex, UK, 2009; pp. 3–28, ISBN 9780470065327.
2. Celii, F.G.; Butler, J.E. Diamond chemical vapor deposition. *Annu. Rev. Phys. Chern.* **1991**, *42*, 643–684. [CrossRef]
3. Green, B.M.; Chu, K.K.; Chumbes, E.M.; Smart, J.A.; Shealy, J.R.; Eastman, L.F. The effect of surface passivation on the microwave characteristics of undoped AlGaN/GaN HEMT's. *IEEE Electron Device Lett.* **2000**, *21*, 268–270. [CrossRef]
4. Wu, Y.F.; Kapolnek, D.; Ibbetson, J.P.; Parikh, P.; Keller, B.P.; Mishra, U.K. Very-high power density AlGaN/GaN HEMTs. *IEEE Trans. Electron Devices* **2001**, *48*, 586–590.
5. Chung, J.W.; Hoke, W.E.; Chumbes, E.M.; Palacios, T. AlGaN/GaN HEMT with 300-GHz fmax. *IEEE Electron Device Lett.* **2010**, *31*, 195–197. [CrossRef]
6. Mishra, U.K.; Parikh, P.; Wu, Y.F. AlGaN/GaN HEMTs—An overview of device operation and applications. *Proc. IEEE* **2002**, *90*, 1022–1031. [CrossRef]
7. Shen, L.; Heikman, S.; Moran, B.; Coffie, R.; Zhang, N.Q.; Buttari, D.; Smorchkova, I.P.; Keller, S.; DenBaars, S.P.; Mishra, U.K. AlGaN/AlN/GaN high-power microwave HEMT. *IEEE Electron Device Lett.* **2001**, *22*, 457–459. [CrossRef]
8. Zheng, X.; Li, H.; Ahmadi, E.; Hestroffer, K.; Guidry, M.; Romanczyk, B.; Wienecke, S.; Keller, S.; Mishra, U.K. High frequency N-polar GaN planar MIS-HEMTs on sapphire with high breakdown and low dispersion. In Proceedings of the 2016 Lester Eastman Conference (LEC), Bethlehem, PA, USA, 2–4 August 2016; IEEE: Bethlehem, PA, USA, 2016; pp. 42–45.
9. Koksaldi, O.S.; Haller, J.; Li, H.; Romanczyk, B.; Guidry, M.; Wienecke, S.; Keller, S.; Mishra, U.K. N-Polar GaN HEMTs exhibiting record breakdown voltage over 2000 v and Low Dynamic On-Resistance. *IEEE Electron Device Lett.* **2018**, *39*, 1014–1017. [CrossRef]
10. Wong, M.H.; Keller, S.; Dasgupta, N.S.; Denninghoff, D.J.; Kolluri, S.; Brown, D.F.; Lu, J.; Fichtenbaum, N.A.; Ahmadi, E.; Singisetti, U.; et al. N-polar GaN epitaxy and high electron mobility transistors. *Semicond. Sci. Technol.* **2013**, *28*, 074009. [CrossRef]
11. Wienecke, S.; Romanczyk, B.; Guidry, M.; Li, H.; Ahmadi, E.; Hestroffer, K.; Zheng, X.; Keller, S.; Mishra, U.K. N-polar GaN cap MISHEMT with Record Power Density Exceeding 6.5 W/mm at 94 GHz. *IEEE Electron Device Lett.* **2017**, *38*, 359–362. [CrossRef]
12. Gaska, R.; Osinsky, A.; Yang, J.W.; Shur, M.S. Self-heating in high-power AlGaN-GaN HFET's. *IEEE Electron Device Lett.* **1998**, *19*, 89–91. [CrossRef]
13. Wang, X.D.; Hu, W.D.; Chen, X.S.; Lu, W. The study of self-heating and hot-electron effects for AlGaN/GaN double-channel HEMTs. *IEEE Trans. Electron Devices* **2012**, *59*, 1393–1401. [CrossRef]
14. Kuball, M.; Hayes, J.M.; Uren, M.J.; Martin, T.; Birbeck, J.C.H.; Balmer, R.S.; Hughes, B.T. Measurement of temperature in active high-power AlGaN/GaN HFETs using Raman spectroscopy. *IEEE Electron Device Lett.* **2002**, *23*, 7–9. [CrossRef]

15. Kolluri, S.; Keller, S.; Denbaars, S.P.; Mishra, U.K. N-polar GaN MIS-HEMTs with a 12.1-W/mm continuous-wave output power density at 4 GHz on sapphire substrate. *IEEE Electron Device Lett.* **2011**, *32*, 635–637. [CrossRef]
16. Jessen, G.H.; Gillespie, J.K.; Via, G.D.; Crespo, A.; Langley, D.; Wasserbauer, J.; Faili, F.; Francis, D.; Babic, D.; Ejeckam, F.; et al. AlGaN/GaN HEMT on diamond technology demonstration. In Proceedings of the Technical Digest—IEEE Compound Semiconductor Integrated Circuit Symposium (CSICS), San Antonio, TX, USA, 12–15 November 2006; pp. 271–274.
17. Dumka, D.C.; Chou, T.M.; Jimenez, J.L.; Fanning, D.M.; Francis, D.; Faili, F.; Ejeckam, F.; Bernardoni, M.; Pomeroy, J.W.; Kuball, M. Electrical and thermal performance of AlGaN/GaN HEMTs on diamond substrate for RF applications. In Proceedings of the 2013 IEEE Compound Semiconductor Integrated Circuit Symposium (CSICS), Monterey, CA, USA, 13–16 October 2013; IEEE: Monterey, CA, USA, 2013; pp. 1–4.
18. Ohki, T.; Yamada, A.; Minoura, Y.; Makiyama, K.; Kotani, J.; Ozaki, S.; Sato, M.; Okamoto, N.; Joshin, K.; Nakamura, N. An over 20-W/mm S-Band InAlGaN/GaN HEMT with SiC/Diamond-Bonded Heat Spreader. *IEEE Electron Device Lett.* **2019**, *40*, 287–290. [CrossRef]
19. Alomari, M.; Dipalo, M.; Rossi, S.; Diforte-Poisson, M.A.; Delage, S.; Carlin, J.F.; Grandjean, N.; Gaquiere, C.; Toth, L.; Pecz, B.; et al. Diamond overgrown InAlN/GaN HEMT. *Diam. Relat. Mater.* **2011**, *20*, 604–608. [CrossRef]
20. Anderson, T.J.; Koehler, A.D.; Hobart, K.D.; Tadjer, M.J.; Feygelson, T.I.; Hite, J.K.; Pate, B.B.; Kub, F.J.; Eddy, C.R. Nanocrystalline diamond-gated AlGaN/GaN HEMT. *IEEE Electron Device Lett.* **2013**, *34*, 1382–1384. [CrossRef]
21. Tadjer, M.J.; Anderson, T.J.; Hobart, K.D.; Feygelson, T.I.; Caldwell, J.D.; Eddy, C.R.; Kub, F.J.; Butler, J.E.; Pate, B.; Melngailis, J. Reduced self-heating in AlGaN/GaN HEMTs using nanocrystalline diamond heat-spreading films. *IEEE Electron Device Lett.* **2012**, *33*, 23–25. [CrossRef]
22. Zhou, Y.; Ramaneti, R.; Anaya, J.; Korneychuk, S.; Derluyn, J.; Sun, H.; Pomeroy, J.; Verbeeck, J.; Haenen, K.; Kuball, M. Thermal characterization of polycrystalline diamond thin film heat spreaders grown on GaN HEMTs. *Appl. Phys. Lett.* **2017**, *111*. [CrossRef]
23. Liu, H.; Li, J.; Li, Z.; Xu, K.; Chen, Z.; Chen, G. Single Crystal Diamond Deposited by Dual Radio-Frequency Plasma Jet CVD with High Growth Rate. *Crystals* **2019**, *9*, 32. [CrossRef]
24. Wang, Q.; Wu, G.; Liu, S.; Gan, Z.; Yang, B.; Pan, J. Simulation-Based Development of a new cylindrical-cavity microwave-plasma reactor for diamond-film synthesis. *Crystals* **2019**, *9*, 320. [CrossRef]
25. Ashkinazi, E.E.; Khmelnitskii, R.A.; Sedov, V.S.; Khomich, A.A.; Khomich, A.V.; Ralchenko, V.G. Morphology of diamond layers grown on different facets of single crystal diamond substrates by a microwave plasma CVD in CH_4-H_2-N_2 gas mixtures. *Crystals* **2017**, *7*, 166. [CrossRef]
26. Yates, L.; Anderson, J.; Gu, X.; Lee, C.; Bai, T.; Mecklenburg, M.; Aoki, T.; Goorsky, M.S.; Kuball, M.; Piner, E.L.; et al. Low thermal boundary resistance interfaces for GaN-On-Diamond devices. *ACS Appl. Mater. Interfaces* **2018**, *10*, 24302–24309. [CrossRef] [PubMed]
27. Zou, Y.S.; Yang, Y.; Chong, Y.M.; Ye, Q.; He, B.; Yao, Z.Q.; Zhang, W.J.; Lee, S.T.; Cai, Y.; Chu, H.S. Chemical vapor deposition of diamond films on patterned GaN substrates via a thin silicon nitride protective layer. *Cryst. Growth Des.* **2008**, *8*, 1770–1773. [CrossRef]
28. Seelmann-eggebert, M.; Meisen, P.; Schaudel, F.; Koidl, P.; Vescan, A. Heat-spreading diamond films for GaN-based high-power transistor devices. *Diam. Relat. Mater.* **2001**, *10*, 744–749. [CrossRef]
29. Graebner, J.E.; Jin, S.; Kammlott, G.W.; Herbt, J.A.; Gardiniert, C.F. Large anisotropic thermal conductivity in synthetic diamond films. *Nature* **1992**, *359*, 401–403. [CrossRef]
30. Sood, A.; Cho, J.; Hobart, K.D.; Feygelson, T.I.; Pate, B.B.; Asheghi, M.; Cahill, D.G.; Goodson, K.E. Anisotropic and inhomogeneous thermal conduction in suspended thin-film polycrystalline diamond. *J. Appl. Phys.* **2016**, *119*, 175103. [CrossRef]
31. Angadi, M.A.; Watanabe, T.; Bodapati, A.; Xiao, X.; Auciello, O.; Carlisle, J.A.; Eastman, J.A.; Keblinski, P.; Schelling, P.K.; Phillpot, S.R. Thermal transport and grain boundary conductance in ultrananocrystalline diamond thin films. *J. Appl. Phys.* **2006**, *99*. [CrossRef]
32. Guillemet, T.; Xie, Z.Q.; Zhou, Y.S.; Park, J.B.; Veillere, A.; Xiong, W.; Heintz, J.M.; Silvain, J.F.; Chandra, N.; Lu, Y.F. Stress and phase purity analyses of diamond films deposited through laser-assisted combustion synthesis. *ACS Appl. Mater. Interfaces* **2011**, *3*, 4120–4125. [CrossRef]

33. Keller, S.; Parish, G.; Fini, P.T.; Heikman, S.; Chen, C.H.; Zhang, N.; DenBaars, S.P.; Mishra, U.K.; Wu, Y.F. Metalorganic chemical vapor deposition of high mobility AlGaN/GaN heterostructures. *J. Appl. Phys.* **1999**, *86*, 5850–5857. [CrossRef]
34. Keller, S.; Li, H.; Laurent, M.; Hu, Y.; Pfaff, N.; Lu, J.; Brown, D.F.; Fichtenbaum, N.A.; Speck, J.S.; Denbaars, S.P.; et al. Recent progress in metal-organic chemical vapor deposition of N-polar group-III nitrides. *Semicond. Sci. Technol.* **2014**, *29*, 113001. [CrossRef]
35. Girard, H.A.; Perruchas, S.; Gesset, C.; Chaigneau, M.; Vieille, L.; Arnault, J.C.; Bergonzo, P.; Boilot, J.P.; Gacoin, T. Electrostatic grafting of diamond nanoparticles: A versatile route to nanocrystalline diamond thin films. *ACS Appl. Mater. Interfaces* **2009**, *1*, 2738–2746. [CrossRef] [PubMed]
36. Laurent, M.A.; Malakoutian, M.; Chowdhury, S. A study on the nucleation and MPCVD growth of thin, dense, and contiguous nanocrystalline diamond films on bare and Si_3N_4-coated N-polar GaN. *Submitt. Semicond. Sci. Technol.* **2019**.
37. Thomas, E.L.H.; Mandal, S.; Ashek-I-Ahmed; MacDonald, J.E.; Dane, T.G.; Rawle, J.; Cheng, C.L.; Williams, O.A. Spectroscopic ellipsometry of nanocrystalline diamond film growth. *ACS Omega* **2017**, *2*, 6715–6727. [CrossRef] [PubMed]
38. Sternschulte, H.; Bauer, T.; Schreck, M.; Stritzker, B. Comparison of MWPCVD diamond growth at low and high process gas pressures. *Diam. Relat. Mater.* **2006**, *15*, 542–547. [CrossRef]
39. Drift, A. Van der Evolutionary selection, a principle governing growth orientation in vapour-deposited layers. *Philips Res. Rep.* **1967**, *22*, 267–288.
40. Chen, Y.C.; Chang, L. Chemical vapor deposition of diamond on an adamantane-coated sapphire substrate. *RSC Adv.* **2014**, *4*, 18945–18950. [CrossRef]
41. Osswald, S.; Mochalin, V.N.; Havel, M.; Yushin, G.; Gogotsi, Y. Phonon confinement effects in the Raman spectrum of nanodiamond. *Phys. Rev. B-Condens. Matter Mater. Phys.* **2009**, *80*, 075419. [CrossRef]
42. Williams, O.A.; Nesladek, M.; Daenen, M.; Michaelson, S.; Hoffman, A.; Osawa, E.; Haenen, K.; Jackman, R.B. Growth, electronic properties and applications of nanodiamond. *Diam. Relat. Mater.* **2008**, *17*, 1080–1088. [CrossRef]
43. Pimenta, M.A.; Dresselhaus, G.; Dresselhaus, M.S.; Cancado, L.G.; Jorio, A.; Saito, R. Studying disorder in graphite-based systems by Raman spectroscopy. *Phys. Chem. Chem. Phys.* **2007**, *9*, 1276–1291. [CrossRef]
44. Eckert, M.; Neyts, E.; Bogaerts, A. Insights into the growth of (ultra)nanocrystalline diamond by combined molecular dynamics and Monte Carlo simulations. *Cryst. Growth Des.* **2010**, *10*, 3005–3021. [CrossRef]
45. Tu, R.; Xu, T.; Li, D.; Zhang, S.; Yang, M.; Li, Q.; Zhang, L.; Shimada, T.; Goto, T.; Shi, J. Morphology and mechanical behavior of diamond films fabricated by IH-MPCVD. *RSC Adv.* **2018**, *8*, 16061–16068. [CrossRef]
46. Wada, N.; Solin, S.A. Raman efficiency measurements of graphite. *Phys. B + C* **1981**, *105*, 353–356. [CrossRef]
47. Shroder, R.E.; Nemanich, R.J.; Glass, J.T. Analysis ofthe composite structures in diamond thin films by Raman spectroscopy. *Phys. Rev. B* **1990**, *41*, 3738–3745. [CrossRef] [PubMed]
48. Fortunato, W.; Chiquito, A.J.; Galzerani, J.C.; Moro, J.R. Crystalline quality and phase purity of CVD diamond films studied by Raman spectroscopy. *J. Mater. Sci.* **2007**, *42*, 7331–7336. [CrossRef]
49. Ager, J.W.; Drory, M.D. Quantitative measurement of residual biaxial stress by Raman spectroscopy in diamond grown on a Ti alloy by chemical vapor deposition. *Phys. Rev. B* **1993**, *48*, 2601–2607. [CrossRef] [PubMed]